Analysis of a Modular Engine Air Particle Separator for use in Unmanned Aerial Vehicles

Marcos Robles[1], Dr. Rasim Guldiken[2]

Abstract
Combat military unmanned aerial vehicles are routinely deployed in dusty parts of the world such as deserts. These particles are harmful to the performance of internal combustion engines used in these UAVs. An engine air particle separator is designed and analyzed using finite element analysis and computational fluid dynamics. This original design features inertial particle separation technology. Initial findings did not report a particle separation efficiency of but did show a maximum pressure of $15.18psi$ with a pressure difference of $1.12psi$. The weight and drag of the EAPS was found to be $23lb$ and $10lb$ respectively. Results show the current design is not suitable for flight and needs to be extensively redesigned such as the vortex blade sweepback. A thorough design of experiment on blade parameters is an area to consider for further investigation.

Keywords
3D Printing — Modular — Optimization — Centrifugal — Particle — Separation — Aerospace — Military — Aerodynamics — ANSYS — Finite Element Analysis — FEA — Computational Fluid Dynamics — CFD — UAV

[1]**Marcos Robles**: mrobles@mail.usf.edu — *Department of Mechanical Engineering, University of South Florida, Tampa, FL, USA*
[2]**Rasim Guldiken**: guldiken@usf.edu — *Department of Mechanical Engineering, University of South Florida, Tampa, FL, USA*

Contents

Introduction

The United States Air Force Research Laboratory (AFRL) has put on a public challenge for students pursuing an engineering degree at an ABET[1] accredited university. The challenge chosen is to design a Modular engine air particle separator (EAPS) for use in military combat unmanned aerial vehicles (UAVs). These UAVs are powered via an internal combustion engine (ICE) which requires clean air to enter the engine inlet for maximum performance and reliability. However, UAVs are frequently deployed in sandy and dusty parts of the world where particles can cause permanent engine damage, decrease engine performance, and decrease the overall reliability of the UAV [1].

The AFRL has placed three design requirements. First, it must be modular so operators and flight crew can easily attach and detach the EAPS from the UAV depending on the environment its in. Second, a very limited number of EAPSs will be produced, therefore, to keep tooling and manufacturing cost to a minimum the EAPS must be manufactured by an additive manufacturing process (AM) chosen by the student. Third, the EAPS must fit inside a volume of 6"x6" and 8" in the axial flow direction and connect to a 1.5" long by 2.5" diameter air intake collar.

Catia V5[2] is used to model the EAPS, ANSYS 16.0 Workbench[3] is used to perform finite element analysis (FEA) and computational fluid dynamics (CFD). Structural analysis will determine if the EAPS is structurally fit for flight. Some important characteristics of this are stress, fatigue, and natural frequencies. CFD will determine if the particle separation is efficient. Some important characteristics of this are pressure drop, air velocity, and drag.

[1] Accreditation Board for Engineering and Technology

[2] Dassault Systemes©2015
[3] ANSYS©2015

1. Background

1.1 Additive Manufacturing

Additive manufacturing (AM) has been an increasingly popular choice for manufacturing components and parts in the aerospace industry. The main benefit of this manufacturing process is that it is cheaper, faster, and easier to use when compared against traditional manufacturing methods such as CNC[4] machining.

From this process, no tooling or fixtures are required as is usually the case for a machining process. This significantly reduces the upfront cost. In addition, there is no time required to set up tooling or program a machine. The only time required is for the software to create an extrusion path and the time it takes to create the part itself.

The AM software and machines are intuitive and easy to use, even for the non-engineer. There are different types of additive manufacturing processes, some of these systems are listed below [2]. There are still new developments and technologies coming from the AM industry. ASTM[5] has already established some standards for additive manufacturing [3].

- Fused Deposition Modeling (FDM)
- Robocasting
- Electron Beam Freeform Fabrication (EBF)
- Direct Metal Laser Sintering (DMLS)
- Electron-Beam Melting (EBM)
- Selective Laser Melting (SLM)
- Selective Heat Sintering (SHS)
- Selective Laser Sintering (SLS)
- Plaster Based 3D Printing (PP)
- Laminated Object Manufacturing (LOM)
- Stereolithography (SLA)
- Digital Light Processing (DLP)

Each of these processes has their own advantages and disadvantages with respect to cost, resolution, manufacturing time, material choice, and the mechanical properties that come from the AM method. For example, titanium can be used in SLS but it has not been extensively used in FDM. Additionally, the direction in which parts are extruded have mechanical property differences [4]. However, parts created using SLS have frequently been used as finished products. For this reason original equipment manufacturers such as Boeing and Airbus use SLS when creating functional parts to be used in flight.

The AM method chosen for this project was Selective Laser Sintering (SLS). The original design and patent for SLS came from The University of Texas created by Dr. Carl Deckard funded by DARPA[6] in 1986 [5]. SLS works by using a high powered carbon dioxide laser to sinter a powered material such as ceramic, metal, or polymer to create a three dimensional part. It does this in layers. With each layer a roller moves across the print area to deposit more of the powdered material. Figure 1 shows a diagram of the process. It should be noted that there exist some alternatives to SLS such as selective laser melting (SLM) and direct metal laser sintering (DMLS). These alternative AM processes provide different mechanical properties and crystal structures compared to SLS.

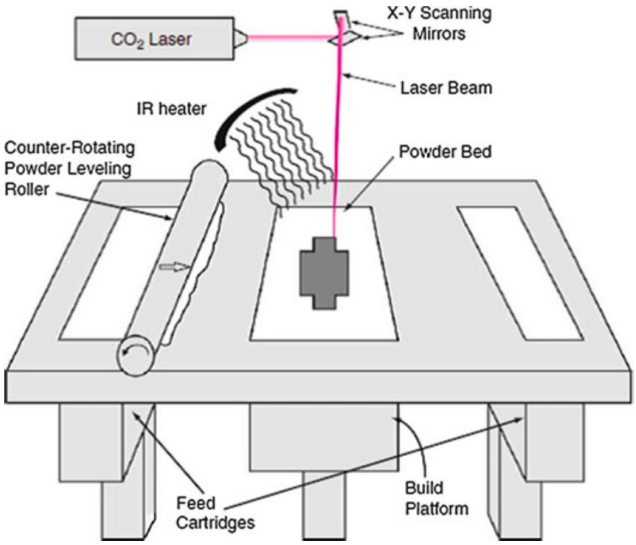

Figure 1. Schematic of the Selective Laser Sintering Process. Courtesy of Gibson [2].

The material selected for this process is a proprietary material from Oxford Performance Materials. Their proprietary OXFAB™ process technology features SLS and advances in material science resulting in desirable mechanical properties for this project [6]. These mechanical properties were used to create a custom material in ASYS for analysis. Even though OXFAB™ was selected, there are many other suppliers and materials to choose from such as Stratasys Ltd. and 3D Systems Inc. to name a few. It is important to investigate the mechanical properties of the material from the suppliers since most suppliers have a proprietary material with different mechanical properties.

There are many limitations and uncertainties with AM technologies. Since the technology is still in its infancy, extensive material testing is left to be desired. Most companies follow the ASTM standard for testing parts created using AM, however, the standard can not keep up with the ever changing industry. In addition, like most manufacturing processes, AM will not produce a perfect part each time. There exist a variability of performance from one part to the next.

The best way to combat this uncertainty is to perform destructive and non-destructive testing of the part created. This needs to be done with a part closest to the actual size to account for the resolution of the AM process. As mentioned before, the direction in which the part is created will change the mechanical properties so this also needs to be considered for part performance when compared to the analysis. These uncertainties will require that the EAPS have a limited shelf life and operation life.

[4] Computer Numerical Control
[5] American Society for Testing and Materials
[6] Defense Advanced Research Projects Agency

1.2 Fluid Dynamics

The UAV being analyzed is the MQ-9 Reaper manufactured by General Atomics Aeronautical Systems. This UAV is a multi-mission, medium-altitude, long endurance remotely piloted combat and surveillance aircraft [7]. The analysis performed uses the maximum performance characteristics of the UAV as specified by the United States Air Force (USAF) such as a cruising speed of $230mph$ and an altitude of $50,000ft$ operating on a standard day [7].

The weight and aerodynamic drag contribute to the overall performance of the EAPS design. The weight of the EAPS will be an additional load the UAV will have to carry. This will increase the lift to drag ratio, however, the aerodynamic drag will more than offset this benefit.

It is difficult to precisely determine the amount of aerodynamic drag with calculations alone. Factors such as antennas and interference drag can skew results by as much as 10% [8]. Wind tunnel testing is needed to get accurate values, fortunately, there has been past research that can provide empirical data to follow. Due to the shape of the EAPS the drag can be calculated similar to that of a fuselage which is considered a non-aerodynamic surface. The total coefficient of drag of the EAPS is a sum of the different types of drag, as seen in Equation 1.

$$C_D = C_{D_P} + C_{D_i} + \Delta C_{D_C} \tag{1}$$

Where C_D is the total coefficient of drag, C_{D_P} is the coefficient of parasite drag, C_{D_i} is the coefficient of induced drag, and ΔC_{D_C} is the coefficient of compressibility drag. Each drag coefficient will be calculated starting with the coefficient of parasite drag. The parasite drag is the sum of the skin friction and the pressure drag. This is more simply expressed, as seen in Equation 2.

$$\Delta C_{D_P} = \frac{C_f K S_{WET}}{S_{REF}} \tag{2}$$

Where ΔC_{D_P} is the coefficient of parasite drag, C_f is the turbulent skin friction coefficient, K is the form factor, S_{WET} is the wetted area of the EAPS (ft^2), and S_{REF} is the reference area (UAV wing area, assumed to be $450ft^2$). The first step is to determine the Turbulent Skin Friction Coefficient, C_f. Experiments have provided a chart which provides C_f given the Reynold's Number. The Reynold's Number can be calculated using Equation 3.

$$Re = \frac{V_O L}{\nu} \tag{3}$$

Where Re is the Reynold's number, V_O is the initial velocity (ft/s), ν is the kinematic viscosity (ft^2/s), and L is the length of the EAPS and engine intake combined (assumed to be $5ft$). This is a combined length since the EAPS geometry is meant to fit perfectly with the engine intake. It can be considered a single body when attached. From this and Figure 11.2, pp.179, *Fundamentals of Flight* [8], $Re = 2.34 \cdot 10^6$ and $C_f = 0.00375$. Next, the Fineness Ratio, L/D must be obtained as seen in Equation 4.

$$Fineness \quad Ratio = body \frac{L}{D} \tag{4}$$

Where D is the diameter of the EAPS (ft). From this and using Figure 11.4, pp. 183, *Fundamentals of Flight* [8], $L/D = 11.333$ and $K = 1.0625$. When these values are substituted back into Equation 2, $C_{D_P} = 0.0035678$. The coefficient of induced drag and compressibility drag can be seen in Equation 5 and Equation 6 respectively.

$$C_{D_i} = \frac{C_L^2}{\pi \cdot AR \cdot e} \tag{5}$$

$$\Delta C_{D_C} = C_{D_{wave,duetolift}} + C_{D_{wave,t/c}} \tag{6}$$

The EAPS does not generate any lift difference whether the EAPS is attached or detached, therefore, there is no induced drag or compressibility drag. The final drag calculation can be seen in Equation 7 which gives a final value of $D = 10lb$. When compared against the weight of the part, approximately $23lb$, this is drag amount is significant. The performance of the part will have to offset the added drag.

$$D = C_D \frac{1}{2} \rho V^2 S \tag{7}$$

Another important factor to consider in fluid dynamics is the boundary layer. The boundary layer is determined by the skin friction and shear stresses created by the fluid is moving past a solid boundary. The skin friction of AM parts can vary greatly depending on which AM process is used. SLS creates a much better surface finish, thus a lower skin friction, compared to that of FDM. The goal is to minimize the skin friction so that maximum velocity can be obtained. Figure 2 illustrates the boundary layer on a late plate.

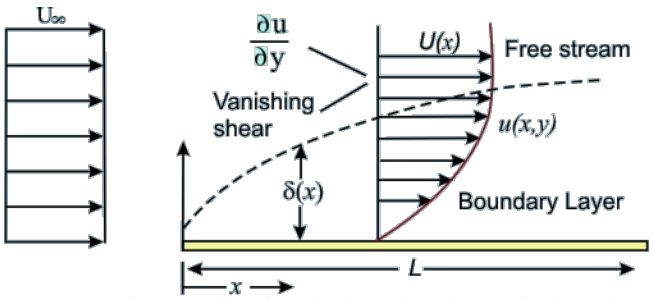

Figure 2. Diagram showing the boundary layer of a late plate. Courtesy of NPTEL [9].

In addition, pressure drop and temperature increase is another consideration of the EAPS. ICEs perform best when there is a steady, cold, high mass flow of air into the intake. Putting an EAPS in front of the inlet will decrease the quality of the air intake. Therefore, the pressure drop across the EAPS is an important parameter to measure. Since the EAPS will create turbulence this will increase temperature, this becomes another important parameter to measure. The particle separation efficiency will have to be weighed against the overall decreased air intake quality.

1.3 Finite Element Analysis

As engineering problems have become increasingly complex, calculating solutions quickly and efficiently has become paramount. FEA has streamlined the engineering process bringing products to market that are more reliable and in a shorter period of time.

FEA works by taking a part geometry and dividing the object into a finite number of smaller elements, each element having a finite number of nodes. Nodes are the points are which a calculation actually takes place. The software then creates a matrix of simultaneous equations to simultaneously solve for the desired parameter. From that first estimation, numerical methods are used to reach the next node on the element and to the other elements. This is repeated until the solution converges.

The elements themselves can take on different shapes. The collection of these elements is referred to as the mesh (see Figure 3). For 2D analysis it can be a triangular or quadrilateral element. For 3D analysis it can be a tetrahedral or more commonly, a brick element. The more complex element shapes provide a more accurate result. However, with this increased complexity comes more nodes and a more complex set of equations to solve. As the number of elements increases so does the number of nodes and the accuracy of the solution. However, with the increased solution accuracy comes an increase in computation time.

The FEA process can be divided into three different steps: pre-processing, FEA solver, and post-processing [10]. Pre-processing consists of building the CAD[7] model, creating a mesh, and then establishing the constraints and loads depending on the application or what is being tested.

Most companies have proprietary numerical methods for obtaining a solution. The distinguishing feature between softwares lies in how accuracy of the results and how efficient they were in obtaining them by having a small computation time and minimizing the computer processor load.

Finally, in post-processing the user gets to decide which results to display, how the display them, and start interpreting the data. The two most important parts of the FEA process are the pre-processing and the post-processing. These also happen to be where there is human intervention. The initial geometry, conditions, or mesh density could be incorrect. The user could also misinterpret results from the solution and not recognize a mistake in the data. This is why a strong understanding of engineering is still required even though the user did not manually compute the solution.

With each of these steps comes a small percent of error that compounds itself by the time a solution is reached. This is why it is critical to validate FEA results with physical testing. FEA provides a great starting point and helps to streamline the engineering process but it is by no means a tool to replace traditional experimentation. Therefore, it becomes necessary the test the EAPS before actual usage.

[7] Computer-aided design

1.4 Computational Fluid Dynamics

The solution for a CFD problem can be solved using the finite volume method, the boundary element method, or the finite difference method [11]. However, the most often used method is the finite difference method. ANSYS gives the ability to chose the method depending on what analysis is being conducted. The Navier-Stokes equations are the main equations used to compute a solution for a model. See Equation 8 for an example of the equation in the x-direction [11].

$$\rho\left(\frac{\partial u}{\partial t}+u\frac{\partial u}{\partial x}+v\frac{\partial u}{\partial y}+w\frac{\partial u}{\partial z}\right)= -\frac{\partial p}{\partial x}+\rho g_x+\mu\left(\frac{\partial^2 u}{\partial x^2}+\frac{\partial^2 u}{\partial y^2}+\frac{\partial^2 u}{\partial z^2}\right) \quad (8)$$

The main difference of FEA and CFD is that the fluid is what needs to be modeled. The easiest way to to do this is create a volume that fills the space you are trying to analyze. It is all the space the object does not take up. Therefore, further pre-processing is required for most CFD studies since it starts with a solid model.

In addition, The boundary conditions are the most important part of the pre-processing stage. There must be long inlet and outlet conditions, typically 10-20 times the volume of the part being analyzed [12]. Without this, the algorithm can not converge on a solution or the solution will be incorrect. This is also why specifying no slip walls or skin friction is important.

Having two particles in the same system creates a unique and complex problem to solve for. Al Makky [13] has created a process for setting up these types of analyses. CFD Online [14] has an extensive library for CFD methods depending on the application. ANSYS has two solvers for CFD, Fluent™and CFX™. Both are used for analysis however, each has their own strengths and weaknesses.

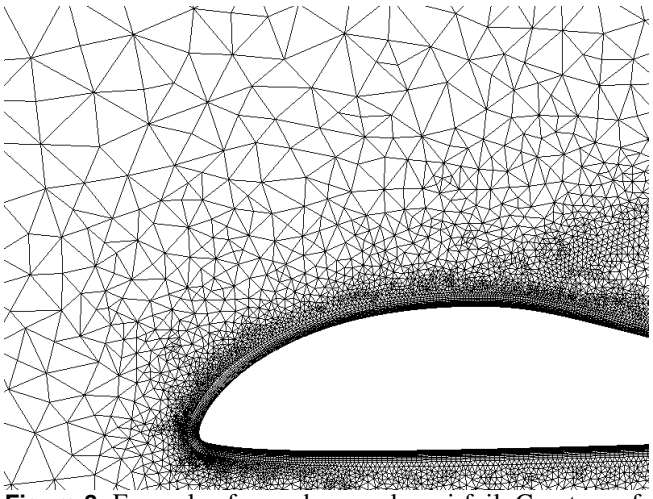

Figure 3. Example of a mesh around an airfoil. Courtesy of Gasparovic [15].

1.5 Particle Separation Technology

The first important consideration is the particle itself. The behavior of a particle is dependent on its density, concentration, shape/form, size distribution, size spatial extent, surface characteristics, and particle/medium interaction (in this case is air). Some processes that affect particle motion are inertial, drag, centrifugal, turbulent, sheer gradient, and coriolis [16]. For this project, the goal is to separate dust and sand from air. According to MIL-STD-810G, particle composition is defined as red china clay where dust is considered to be $< 150\mu m$ and sand is $150\mu m$ to $850\mu m$ in size [17].

There exist many different technologies for separating particles. Some of these technologies are listed below. There also exists other methods such as using a serpentine microchannel [18] or a louver particle separator [19]. However the main types of EAPSs are typically found in helicopters. These are vortex tube separators (VTS), inertial particle separators (IPS), and inlet barrier filters (IBS). Examples of these systems can be seen in Figure 4, 5, and 6 respectively.

- Sieving
- Gravitational Sedimentation
- Centrifugal Sedimentation
- Elutriation
- Electrostatic Precipitation
- Thermal Precipitation
- Impaction
- Hydrodynamic Chromatography (HDC)

The most recent development of an IPS is from a patent Honeywell applied for in February 2015 [20]. There even exist commercial products of VTS such as those from Donaldson Company Inc. [21] achieving separation efficiencies up to 99%.

The main performance characteristics of an EAPS are grade efficiency, overall separation efficiency, pressure drop, power consumed, lifetime improvement, and engine power deterioration [22]. Some additional characteristics are weight, drag, and frontal area [23]. VTS has a low pressure drop, IBF has a low change of inlet mass flow rate, but all methods still degrade due to clogging and erosion [22] [23]. Since the challenge calls for an AM process the IBS can not be considered. The VTS outperformed the IPS therefore the goal becomes designing a modular VTS.

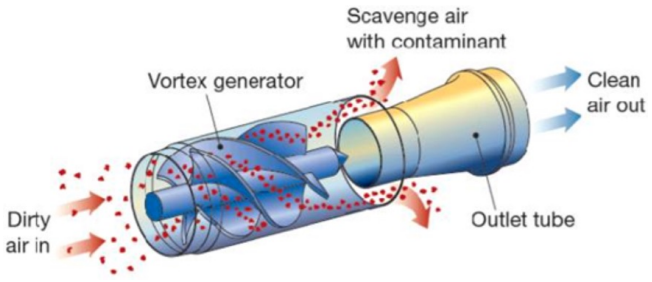

Figure 4. Illustration of a VTS. Courtesy of Pall [24].

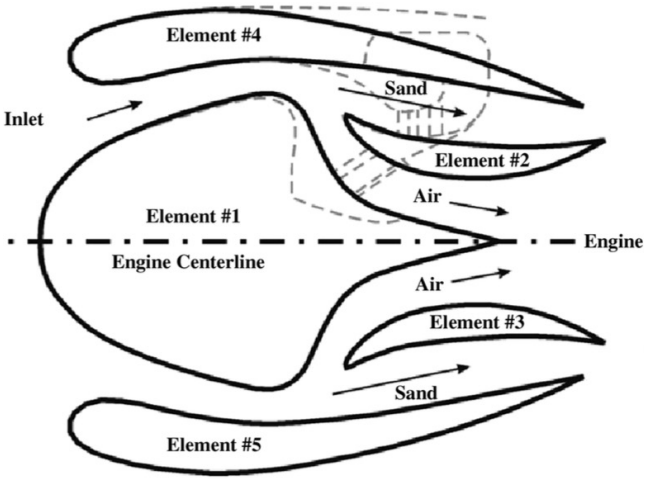

Figure 5. Illustration of an IPS. Courtesy of Al-Faris [25].

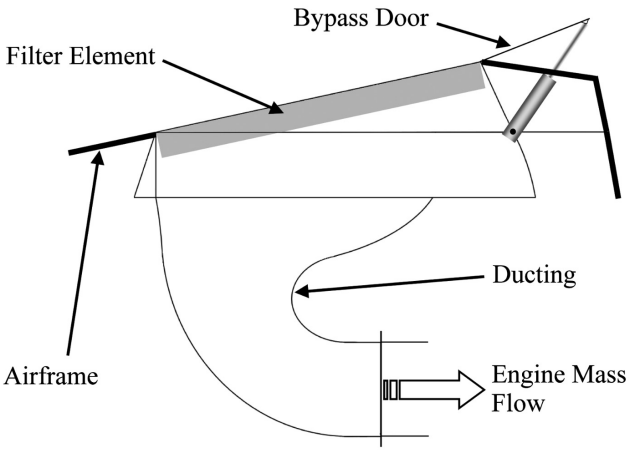

Figure 6. Illustration of an IBF. Courtesy of Bojdo [22].

A theory for particle separation efficiency for a VTS has already been proved and provided by Ramachandran et al. [26] and can be seen in Equation 9. Where Q_g is the tube volume flaw rate, x is the particle diameter, R_{co} is the radius of the collector, H_t is the helix pitch, and L_v is the length of the separating region.

$$E(x)_{VTS} = 1 - exp\left(- Q_g \frac{8\pi}{18\mu_g} x^2 \frac{L_v}{R_{co}^2 H_t^2} \right) \tag{9}$$

Further, Bojdo and Filippone [22] have developed equations that will calculate the pressure drop across the VTS for the core region and the scavenge region. VTS has already been employed and used in helicopters such as those in MD Helicopters, Inc. [27]. Sometimes, VTSs are combined together in an array to fill as much of the frontal area of an engine inlet. The disadvantage of doing this is that there are gaps between each VTS that only add drag to the system.

Even though though VTS will be the technology of choice it is important no note that VTS will not work for every application. In fact, engine performance and characteristics are frequently changed to compensate for the addition of an EAPS, however, this will not be the case for this application.

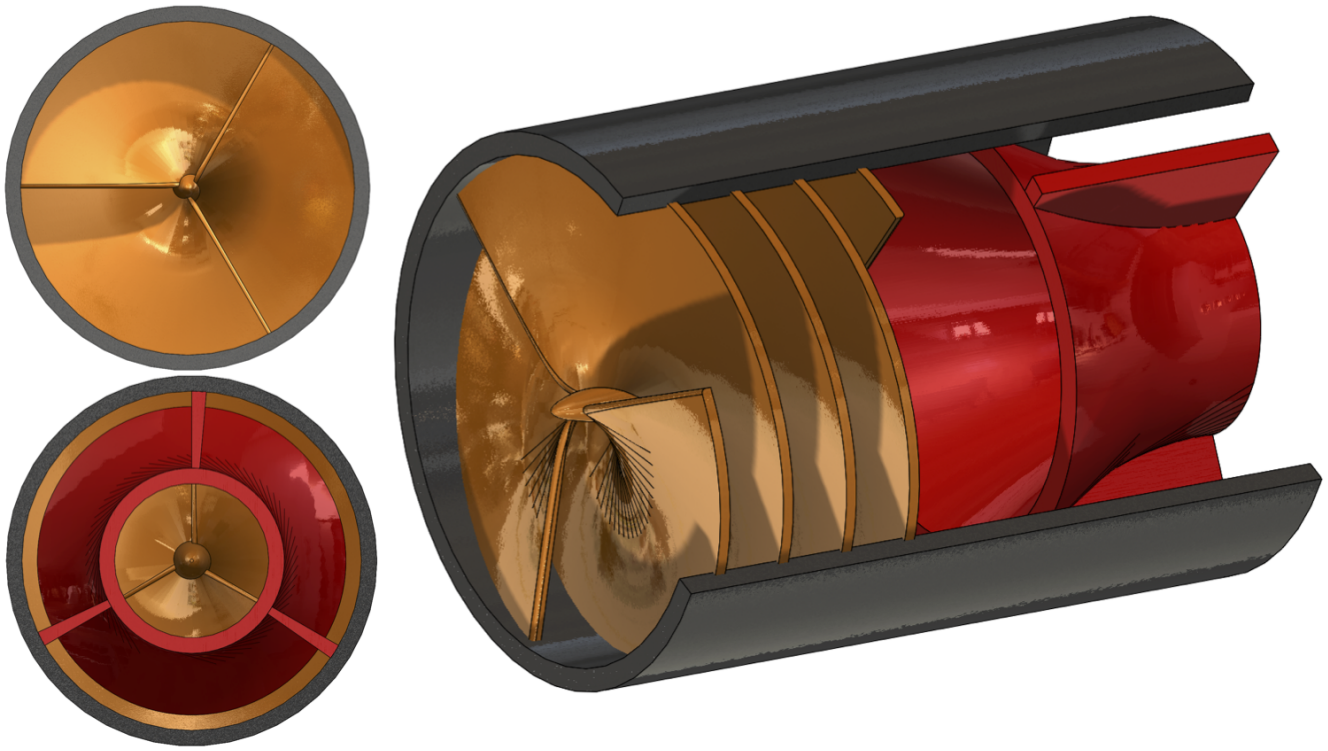

Figure 7. Rendering of the originally designed EAPS with colored sections to distinguish each feature. The EAPS shroud is in black, the vortex is in orange, and the collector with its supports is in red. The top left picture is a front view and the bottom left picture is a rear view. (Portion of the shroud cut to allow visibility inside the EAPS)

2. Design

The overall design of the EAPS is similar to that of a VTS. It has simply been scaled up to fill the volume as specified by the AFRL student challenge. Since this part is meant to be manufactured via SLS, the entire EAPS will print as one part regardless of how the VTS is sectioned. The thickness of the vortex blades will attached to the wall of the shroud. Similarly, the collector supports also attach to the shroud wall. The shroud diameter is 6". Figure 7 shows the EAPS design.

The end of the vortex blades are rounded such that it mimics an air foil to decrease turbulence and drag as the fluid exits the vortex section. The thickness of the vortex blades are $1/8$". All other features of the EAPS are $1/4$" thick. An initial number of 3 blades was chosen for the EAPS. In addition, the length of the vortex 3" and the helix has 1.25 rotations.

The center of the vortex features 4" long convex cylinder. This cylinder serves multiple purposes. It is meant to reduce drag since it has a laminar shape. In addition, it helps the EAPS achieve higher separation efficiency. Finally, the center piece adds stability to the vortex. The EAPS has a separating region of 1.75". Figure 8 shows the separation region.

The collector features a loft that transitions from a 4.5" inside diameter to a 2.5" inside diameter. This will maximize the amount of air that is collected. It will also streamline the air and create a higher pressure. As mentioned before, having a low drop in pressure will add to the overall performance of the EAPS.

Some important parameters to be evaluated for research are the length of the separating region, length of the vortex region, vortex fin pitch, loft geometry, collector length, center piece thickness an length, and finally, the thickness of all the features.

This design has a calculated drag of $10lb$ and an overall weight of $23lb$. Therefore, the EAPS adds a weight of $33lb$, an important consideration for overall UAV performance.

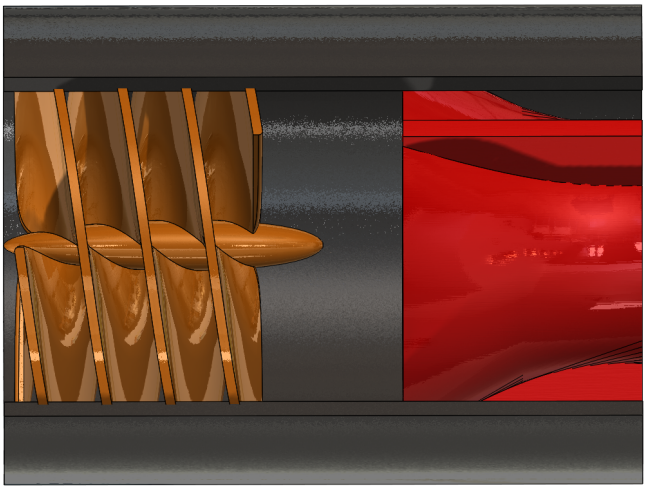

Figure 8. Side rendering of the EAPS with separating region in the center. The air-particle mixture enters from the left. (Portion of the shroud cut to allow visibility inside the EAPS)

Figure 9. Mesh of the fluid volume used in the CFD analysis. The point in the center is where the EAPS is. It features a more dense mesh in that area due to the complex geometry.

3. Analysis

3.1 Finite Element Analysis Set Up

The OXFAB^{TM} material properties were imported in ANSYS based upon the data provided by Oxford Performance Materials. An automatic fine mesh was created using ANSYS. An initial analysis showing structural error was performed. From the results a mesh refinement was placed along the edge of the vortex that connects with the center piece since this showed the most probable area of error.

A fixed support was placed at the rear of the collector. This simulates how the EAPS is connected to the 2.5" diameter by 1.5" long engine air intake as specified by the challenge. A dynamic pressure was calculated based upon a worst case scenario. This suggests the UAV is experiencing an altitude density of $0.0023769 slugs/ft^3$ (at sea level) and a velocity of $230 mph$. This resulted in a dynamic pressure of $1.15 psi$.

This pressure was applied to the entire surface of the blades and the front of the shroud. This is not reflective of the actual pressure distribution, however, it acts as a safety factor creating an excess of stress on the part. A modal analysis was also run. There were no fixed supports in this analysis to determine the natural frequencies of the part. This is important to see if it will respond with the frequencies generated by the engine.

Neither a fatigue nor temperature analysis could be performed since the fracture, fatigue and temperature information of the material properties are not provided. This would have tested the fracture toughness of the EAPS as well as the thermal response to varying temperatures changes that occur when changing altitude. This creates a cyclic stress that should be accounted for.

3.2 Computational Fluid Dynamics Set Up

The EAPS was first enclosed in a large cylinder. With respect to the center of the EAPS, the cylinder created measured 12" in diameter, 36" in length towards the front and 50" in length towards the rear. This creates a large volume for the computations to take place. As mentioned before, it is important to create very large boundaries to hold the accuracy of the simulation. Failure to do so would create false results.

Once the cylinder was created a boolean tool in ANSYS was used to subtract the EAPS volume from the cylinder volume. This created a volume of where only the air exist. The hollow space now was only where the EAPS used to be. This now becomes the fluid volume where the air will flow. An automatic fine mesh was used to create the elements and nodes of the fluid volume as seen in Figure 9.

For the analysis set up there was a velocity inlet and a pressure outlet. This is frequently the best way to converge on a solution and run an analysis [28]. The velocity inlet was chosen as air at $25C$ with a velocity of $230 mph$ at a turbulence option of medium (turbulence $= 5\%$) and the pressure outlet was chosen to be an average pressure of $1 atm$. The inlet face was picked at the front of the cylinder and the outlet was chosen as the rear of the cylinder.

The opening setting was also chosen as $1 atm$ and the location was the cylindrical face of the cylinder. The wall was all parts of the EAPS surface and geometry. The settings were left as default for a no slip wall and left as a smooth wall. However, the SLS does not leave a perfect surface finish on the part. This is one inaccuracy from the analysis.

A steady state solution was solved using ANSYS CFX©. Particles could not be accurately added for air-particle mixture. Further time needs to be spent on the air-particle inlet.

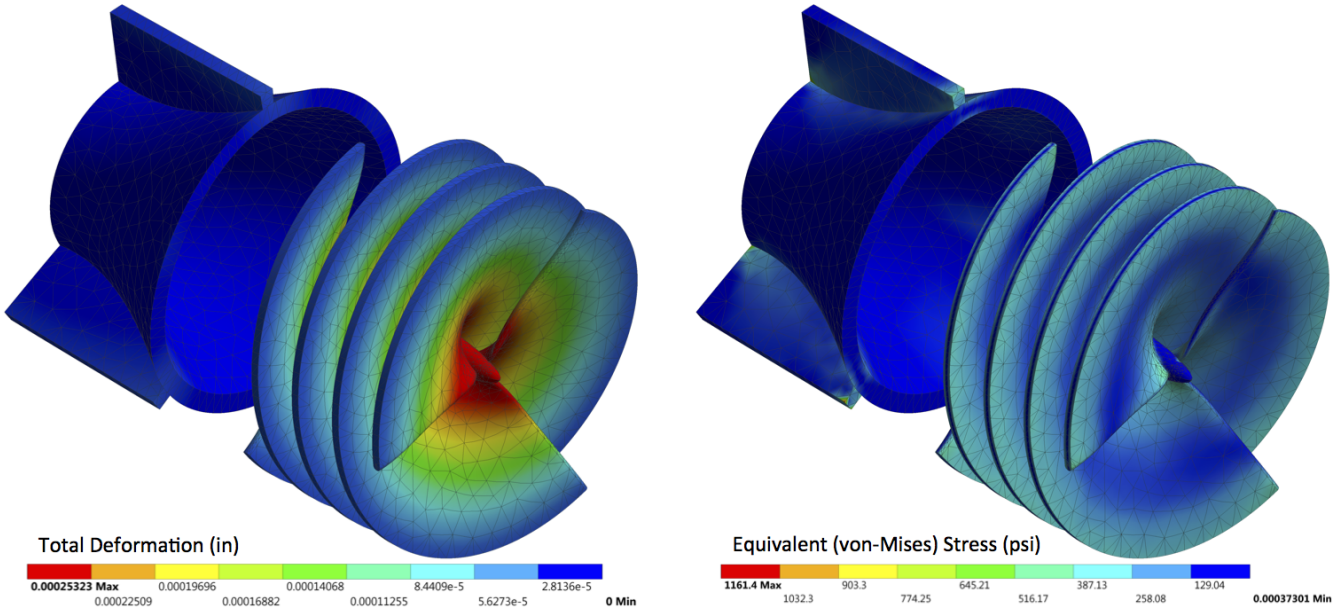

Figure 10. A (left side): Total deformation mesh/contour with a maximum displacement of $253\eta in$ at the the center piece. **B (right side):** Total stress mesh/contour with a maximum stress of $1.161 Ksi$. There was no significant stresses or deformations associated with the shroud. Therefore, the shroud was removed allow visibility inside the EAPS.

4. Results and Discussion

4.1 Finite Element Analysis Results

Based on the analysis the part exceeds the minimum structural requirements with a safety factor of 15. With a maximum displacement of $253\eta in$ and a maximum stress of $1.161 Ksi$ there is a lot of opportunity to reduce the wall thicknesses and reduce weight. In aerospace applications a safety factor of 1.5-3 is desired. However, due to the uncertainties that come with SLS, a safety factor of 3-5 is a more reliable target. Redesigning the wall thicknesses to this safety factor will result in a weight savings greater than 25%.

With doing this there are still areas that can be redesigned. Such areas include the collector supports and the fin connections to the shroud wall and either piece. Placing fillets at these points can considerably reduce the stress concentrations that occur from the sharp geometry change. This can also help to reduce overall weight.

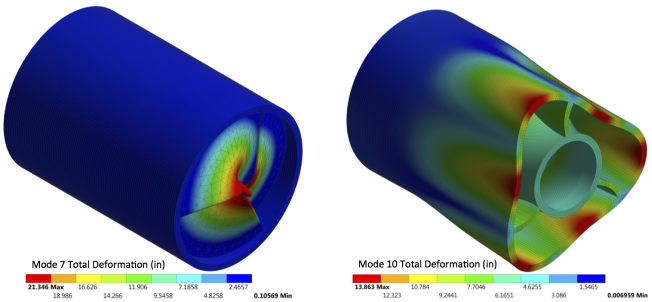

Figure 11. Modal response of the EAPS. **A (left side):** Front view of Mode 7 at $1368.2 Hz$. **B (right side):** Rear view of Mode 10 at $2460.6 Hz$.

The modal analysis revealed a fundamental frequency of $1368.2 Hz$ as seen in Table 1. The fundamental frequency behaved very similarly to the total displacement from the pressure applied. Modes 7-10 behaved similarly to each other with the rear of the shroud deforming the most as seen in Figure 11. This is well below the operating frequencies of the Honeywell TPE331-10GD turboprop engine used in the MQ-9 Reaper [1]. However, the best approach to ensure safety is to perform a harmonic response analysis by applying the frequency ranges of the engine to the EAPS.

Another factor that needs consideration is fatigue. The best way to determine the number of cycles to failure will be to perform physical experimentation since the mechanical properties of the material are still considered unknown. These analyses need to be validated with physical experimentation after the part has been redesigned to a safety factor of 3-5.

Table 1. Table of modes. Modes 1 through 6 do not exist since they represent the initial 6 degrees of freedom.

Mode	Frequency (Hz)
1	–
2	–
3	–
4	–
5	–
6	–
7	1368.2
8	1879.8
9	1880.1
10	2460.6

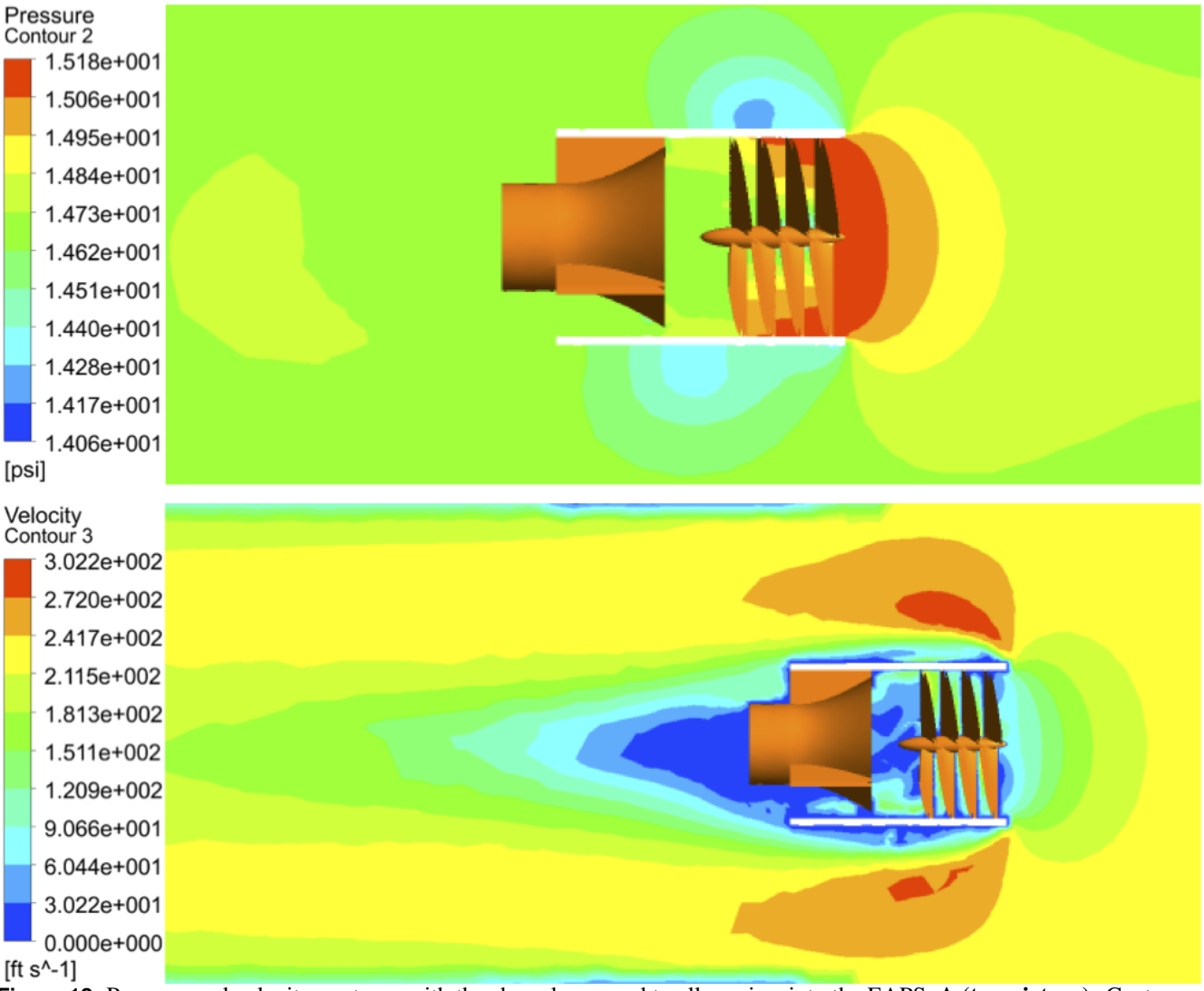

Figure 12. Pressure and velocity contours with the shroud removed to allow view into the EAPS. **A (top picture):** Center plane pressure contour of the EAPS with a maximum pressure of $15.18 psi$. **B (bottom picture):** Center plane velocity contour of the EAPS with a maximum velocity of $302.2 ft/s$.

4.2 Computational Fluid Dynamics Results

Since the air-particle inlet could not be accurately modeled, the results will only focus the effects of air on the EAPS. The EAPS has a maximum pressure at the front of the EAPS where the vortex begins as seen in Figure 12.A. This is the result of a poor design. The blades of the vortex should have a greater sweepback angle. This will give the air a chance to be redirected smoothly without having to make an abrupt change. While it will not completely eliminate the increase in pressure, it will still make a difference. Making this change will decrease the drag as well.

The front and rear edges of the shroud should be curved to make it more aerodynamic. This will help the air flow over the EAPS more easily. The lower pressure areas are a result of the edges of the shroud. However, along the overall length of the EAPS a pressure difference of $1.12 psi$ is obtained. This is a significant amount and needs to be reduced considerably.

Figure 12.B shows the velocity profile of the EAPS. The non-aerodynamic edges have resulted in an increased velocity as seen in red. This is a undesirable effect. In an effective design, the velocity around the outside area of the EAPS will be equal to that of the inlet. In addition, the air leaving the air intake should be equal to the inlet velocity. A drop it expected, however, the results show $0 ft/s$ at the intake. As well, the velocity in the separation section also shows a velocity of $0 ft/s$. This is the result the vortex blades not being sweptback as well as a small separation length. Changing both of these aspects will provide a higher velocity within the EAPS.

The lack of symmetry in the pressure and velocity contours in Figure 12 is the result of the collector supports at the rear. The 3 supports are aligned equally radially. When a plane is created down the center of the EAPS, the effects of the support is seen in the upper portion and the effects of not having the support are towards the bottom of the EAPS.

Figure 13 shows the pressure contour on the surface of the EAPS. The pressure is smaller towards the center of the vortex blades when looking at the front of the blades. When looking at the rear (not pictured), the pressure decreases along the entire face. This is from the pitch of the blades. From the front the blade acts as an inhibitor for fluid motion but the rear acts as an enabler.

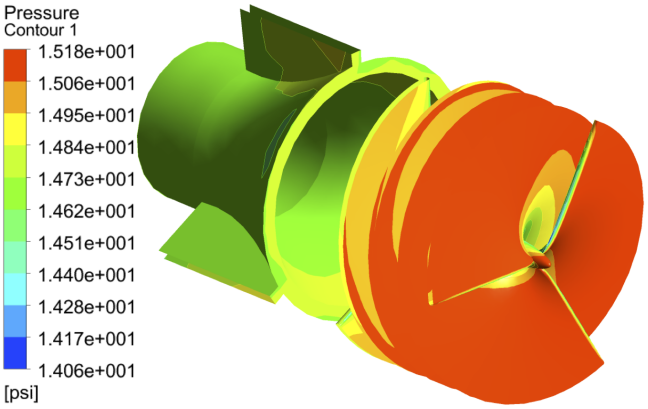

Figure 13. Pressure contour on the EAPS surface with a maximum pressure of 15.18psi.

Figure 14 shows the velocity streamline of the entire EAPS. The lack of sweepback on the vortex blades forces air back towards the outside of the EAPS rather than inside. This causes the air density to increase and then the tightly packed air molecules have to find the easiest path which is around, rather than inside, the EAPS. Even though there are no sand and dust particles major design improvements can be made just to help the air move through and around the EAPS.

Further analysis should be done on varying the sweepback and pitch of the vortex blades to minimize the pressure drop and maximize the engine air intake velocity. From the analysis the blade sweepback is a key design parameter for an effective EAPS as proven by Hobbs [29].

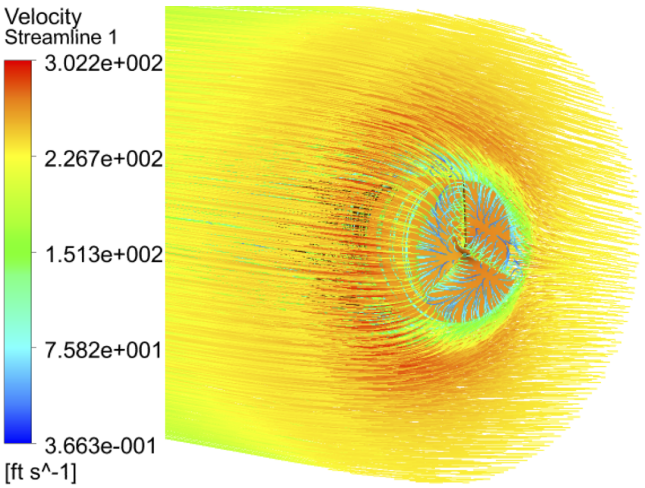

Figure 14. Velocity streamline along the front of the EAPS with a maximum velocity of 302.2ft/s.

5. Conclusion

Even though the particle separation could not be modeled, the FEA and CFD show significant design improvements that can be made. FEA has shown that the stress concentrations around the collector supports and edges of the vortex blades can be relieved to decrease the maximum stress it endures. Further, the FEA also shows that the wall thickness of the EAPS to be reduced to create an overall safety factor between $3-5$ and reduce weight. An important considered is how the forces that the particles exert on the EAPS as shown by Jiang [30].

The CFD results show illuminate the very poorly designed vortex blades. Since there is no sweepback the air can not effectively move to through the EAPS and actually leads to an increase in drag. Further, all the surfaces and edges should be contoured to create aerodynamic surfaces. The analysis leaves much to be desired for future research and investigation. The list below names a few of these key areas.

- Proper loading found from CFD pressure vales
- Fatigue due to:
  - Thermal Expansion
  - Cyclic Loading
  - Particle Impact
- Harmonic Response
- Fracture Mechanics of Particle Impact
- CFD for Various Altitudes
- CFD Solver and Solution Settings
- Physical Experimentation

After all these areas are investigated a design of experiment needs to be performed looking into the key parameters governing the effectiveness of the EAPS such as blade sweepback, vortex pitch, collector area, separation length, and vortex length to name a few.

Acknowledgments

This project has taught me a great deal about the research process, computational fluid dynamics, and the challenges of carrying out a project from start to finish. If I were to do this project again I would drastically change my overall timeline. I realized that the background research should be completed first and foremost. During this process the research topic should be refined to an area that has yet to be explored. Only after that is done should the design process start. In addition, analysis should be been performed early on to detect any initial obvious design flaws the can be changed. Once 3 design iterations are done a final and complete analysis and design of experiment can be performed. Further, the report itself should include more statistics and probabilities include as the analysis.

I would like to thank Dr. Rasim Guldiken for his guidance, advice, and expertise in research and Fluid Dynamics and Dr. Jose Porteiro for his expertise in Aerodynamics.

References

[1] A. F. R. Laboratory. Modular uav engine air particle separator. [Online]. Available: http://www.afrlstudentchallenge.org/AFRLCapstone.nsf/cps/17B369831B543CD885257A670068931D/$FILE/Modular-UAV-EngineAirParticleSeparator-vJuly2013.pdf

[2] B. S. Ian Gibson, David Rosen, *Additive Manufacturing Technologies*, 2nd ed. Springer, 2015.

[3] ASTM. Additive manufacturing technology standards. [Online]. Available: http://www.astm.org/Standards/additive-manufacturing-technology-standards.html

[4] A. Basik, "Mechanical properties of fused deposition modeling parts manufactured with ultem 9085," *ANTEC*, 2011.

[5] C. R. Deckard, "Method and apparatus for producing parts by selective sintering," Board of Regents, The University of Texas System, United States Patent Application US 4863538 A, October 1986.

[6] Oxford performance materials. [Online]. Available: http://www.oxfordpm.com/index.php

[7] U. S. A. Force. (2010, August) Mq-9 reaper. [Online]. Available: http://www.af.mil/AboutUs/FactSheets/Display/tabid/224/Article/104470/mq-9-reaper.aspx

[8] R. S. Shevell, *Fundamentals of Flight*, 2nd ed. Prentice Hall, Inc., 1989.

[9] N. P. on Technology Enhaced Learning. Chapter 9 lecture 28 boundary layer equations. [Online]. Available: http://www.nptel.ac.in/courses/112104118/lecture-28/images/fig28.1.gif

[10] X. Chen and Y. Liu, *Finite Element Modeling and Simulation with ANSYS Workbench*, 1st ed. CRC Press, 2015.

[11] B. R. Munson, *Fundamentals of Fluid Mechanics*, 7th ed., A. P. R. Theodore H. Okiishi, Wade W. Huebsch, Ed. John Wiley and Sons, Inc., 2013.

[12] ANSYS. Fluid dynamics technology tips. [Online]. Available: http://www.ansys.com/Products/Simulation+Technology/Fluid+Dynamics/CFD+Technology+Leadership/Technology+Tips

[13] A. A. Makky. (2015) Computational fluid dynamics is the future. [Online]. Available: http://cfd2012.com/

[14] (2015, April) Cfd online. [Online]. Available: http://www.cfd-online.com/

[15] P. Gasparovic. High lift prediction capability of cfd. [Online]. Available: http://buteo.szm.com/projects/001_ua2/cel.gif

[16] A. I. A. Salama, "Mechanical techniques: Particle size separation," *Natural Resources Canada*, pp. 3277–3289, 1999.

[17] U. S. D. of Defense, "Mil-std-810g," *United States Department of Defense*, vol. Sand and Dust, no. 510.5, pp. 510.5–1–5–13, October 2008.

[18] e. a. Jun Zhang, "Inertial particle separation by differential equilibrium positions in a symmetrical serpentine micro-channel," *Scientific Reports*, vol. 4, 4527, no. DOI 10.1038/srep04527, pp. 1–9, March 2014.

[19] e. a. Grant O. Musgrove, "Computational design of a louver particle separator for gas turbine engines," *ASME Turbo Expo 2009: Power for Land, Sea and Air*, no. 8-12, pp. 1–11, June 2009.

[20] e. a. Zedic Daniel Judd, "Inlet particle separator system with hub and/or shroud suction," Henoywell International Inc., Morristown, NJ, United States Patent Application US 2015/0040535, February 2015.

[21] I. Donaldson Company, "Donaldson inertial particle separation technology," Donaldson Company, Inc. Aerospace and Defense Group, USA, Brochure F111219 ENG, September 2014.

[22] N. Bojdo and A. Filippone, "Comparative study of helicopter engine particle separators," *Journal of Aircraft*, vol. 51, no. 3, pp. 1030–1042, May-June 2014.

[23] N. B. Antonio Filippone, "Turboshaft engine air particl separation," *Progress in Aerospace Sciences*, vol. 46, no. DOI 10.1016/j.paerosci.2010.02.001, pp. 224–245, March 2010.

[24] P. Aerospace, "Introduction to helicopter engine inlet protection," Pall Aerospace, Powerpoint, 2009.

[25] E. F. Al-Faris and F. Saeed, "Design and optimization method for inertial particle separator systems," *Journal of Aircraft*, vol. 46, no. 6, pp. 1919–1929, November-December 2009.

[26] P. R. O. Ramachandran and D. Leith, "Collection efficiency and pressure drop for a rotary-flow cyclone," *Filtration and Separation*, vol. 31, no. 6, pp. 631–636, 1994.

[27] *Engine Air Particle Separator Description and Operation*, 22nd ed., Md Helicopters, Inc.

[28] ANSYS. Simulating the performance of solid cyclone separator. [Online]. Available: http://www.ansys.com/Products/Simulation+Technology/Fluid+Dynamics/CFD+Technology+Leadership/Technology+Tips/Simulating+Solid+Separator+Cyclone

[29] A. Hobbs, "Design and optimization of a vortex particle separator for a hot mix asphalt plant," *ANSYS*, January 2004.

[30] M. Jiang and B. Wang, "Numerical anlylsis of applied forces information exerted on particles in cyclone separators," *AIP Conf. Proc.*, vol. 1547, no. DOI 10.1063/1.4816918, pp. 640–651, 2013.